Available online at www.sciencedirect.com
SCIENCE DIRECT®
Journal of the European Ceramic Society 25 (2005) 3315–3321
www.elsevier.com/locate/jeurceramsoc

Ionic conductivity and microstructure of solid electrolyte $La_2Mo_2O_9$ prepared by spark-plasma sintering

Jianhua Yang*, Zhaoyin Wen, Zhonghua Gu, Dongsheng Yan

Shanghai Institute of Ceramics, Chinese Academy of Sciences, 1295 Dingxi Road, Shanghai, China

Received 11 June 2004; received in revised form 1 August 2004; accepted 15 August 2004
Available online 28 October 2004

Abstract

Dense $La_2Mo_2O_9$ ceramic electrolytes were prepared with ultrafine powder by the SPS rapid sintering method. The conductivity of the specimens by SPS was much higher than those sintered by conventional process. Moreover, the unilateral alignment of rod-type grains happened in the specimens sintered by SPS at higher temperatures or for longer holding time. The anisotropy in ionic conductivity was attribute to the directional alignment of rod-type grains. The oxygen ion conductivity parallel to the direction of rod-type grains was higher than that perpendicular to the grains.

Keywords: $La_2Mo_2O_9$; Spark-plasma sintering; Ionic conductivity

1. Introduction

Oxide conductors with high conductivity of oxygen ion have been attracting considerable interests because of their potential applications in solid oxide fuel cells (SOFC), oxygen pumps, oxygen sensors and oxygen-permeable membrane catalysts.[1–4] The main oxide-ion conductors known to date belong to four distinct structure groups: fluorite type, deficient perovskites, Aurivillius type phases and pyrochlores.[5–8] Among them, the most widely studied and commonly used material is yttria-stablized zirconia (YSZ), which has been successfully used in SOFC and oxygen sensors. But for these traditional oxide conductors, they usually need high working temperatures to achieve a relatively large oxygen flux for efficient operation. In 2000, Lacorre et al.[9] first reported a kind of novel oxide conductor $La_2Mo_2O_9$, which exhibited oxygen ionic conductivity comparable to that of yttria-stablized zirconia. The studies on such compounds have opened a new window in the research of oxide conductors and provided another potential candidate of electrolyte for SOFC and sensor applications. Several methods have been used to prepare $La_2Mo_2O_9$, such as sol–gel method[10] and high-energy ball milling,[11] but these methods are limited in the preparation of $La_2Mo_2O_9$ powder. So far, the conventional sintering method was still applied for the preparation of $La_2Mo_2O_9$ ceramics,[12] which needed several grindings and long period of high temperature sintering. It was difficult to obtain fully dense ceramics by the conventional sintering route, which greatly affected the ionic conductivity of the ceramics.

Spark-plasma sintering (SPS)[13,14] is a relatively new sintering method for rapid consolidation for a variety of ceramic materials in a short sintering time. The versatility of SPS allows very quick densification to near theoretical density for a number of metallic, ceramic and multi-layer materials under a low vacuum environment (∼5 Pa). Typical sintering time can be reduced from 12 h or longer for conventional sintering to less than approximately 30 min for SPS.

In this study, ultrafine $La_2Mo_2O_9$ powder was prepared by a sol–gel method. $La_2Mo_2O_9$ ceramic disks were prepared by SPS sintering. The effects of sintering parameters of SPS on sample microstructure, density and ionic conductivity were

* Corresponding author. Fax: +86 21 5241 3903.
E-mail address: jhyang@sunm.shcnc.ac.cn (J. Yang).

0955-2219/$ – see front matter © 2004 Elsevier Ltd. All rights reserved.
doi:10.1016/j.jeurceramsoc.2004.08.023

investigated and compared with those of conventionally sintered samples.

2. Experimental

Ultrafine $La_2Mo_2O_9$ powders were prepared by a sol–gel method. Lanthanum nitrate $La(NO_3)_3{\cdot}H_2O$ (AR) and ammonium molybdate $(NH_4)_6Mo_7O_{24}{\cdot}4H_2O$ (AR) solutions were prepared separately and then mixed with metallic ions (La/Mo) in the molar ratio of 1:1. Citric acid (AR) solution was then added slowly to the above solution with gentle stirring. The molar ratio of citric acid to total metallic ions was controlled at 0.3. The pH value of the solution was adjusted to 3 by adding HNO_3 solution slowly. The solution was kept in a water bath at 80 °C until gelation was completed, and then the as-prepared gels were dried at 120 °C for 24 h. The ultrafine $La_2Mo_2O_9$ powders were obtained by calcining the dried gel at 500 °C for 4 h. Fig. 1 showed the schematic of the SPS system (Dr. Sinter-2040, Japan) configuration.[15] The ultrafine $La_2Mo_2O_9$ powder was placed in a graphite die (ϕ 10 mm), and the SPS system was evacuated to 5 Pa, then an electric current of ~1000 A was applied through the graphite die. The applied pressure was 45 MPa and the heating rate was set to 100 °C/min. The sintering temperature was in the range of 750–900 °C with a holding time of 0–30 min. The conventional sintering of $La_2Mo_2O_9$ ceramic disc was performed as described in reference.[12] The density of the sintered ceramic $La_2Mo_2O_9$ was measured by the method of mercury filling pressure on a densitometer (Poresizer 9320, Micro-Meritics, USA), and the relative density was therefore calculated by the ratios of the measured density to the theoretical density.[12] The binding energy peak of carbon in the as-sintered SPS $La_2Mo_2O_9$ specimen was observed in the X-ray photoelectron spectrum (Microlab 310F with XPS, USA). The X-ray diffraction patterns of the specimens were recorded at room temperature in the 2θ range of 10–70° (JDX-3500 X-ray diffractometer, JEOL Company, Japan). The particle size of ultrafine powders was observed with a transmission electron microscope (200 kV, JEOL 2010, Japan). The microstructure of the fractured section of the specimens was observed with the scanning electron microscope (JEOL, JSM-6799F, Japan). The ionic conductivity of samples was determined in flowing air and pure oxygen atmosphere by ac impedance spectroscopy in the frequency range of 0.1 Hz to 1000 kHz using a Solartron frequency response analyzer (Solartron SI-1260, England). The specimen for the test was 2 mm in thickness and 10 mm in diameter with platinum electrodes on both flat surfaces formed by sintering Pt paste at 900 °C for 20 min.

3. Results and discussion

The $La_2Mo_2O_9$ ultrafine powder prepared by sol–gel method was milky white. Typical TEM image as shown in Fig. 2 revealed a size distribution of the particles in the range of 20–50 nm. Since graphite was used as the die material in the SPS process, carbon was found to diffuse into the specimen, therefore the specimen obtained by SPS sintering became dark, which may affect the measurement of the electrical properties of the solid electrolyte samples. An apparent 1s binding energy peak of carbon was observed in the X-ray photoelectron spectrum (XPS) for the as-sintered SPS $La_2Mo_2O_9$ specimen as shown in Fig. 3. However, when the specimen was annealed at 700 °C for 2 h in air, the specimen became white, and the carbon 1s binding energy peak disappeared, which indicated that the annealing conditions were effective to eliminate the carbon contamination through SPS process. The XRD pattern of the annealed SPS $La_2Mo_2O_9$

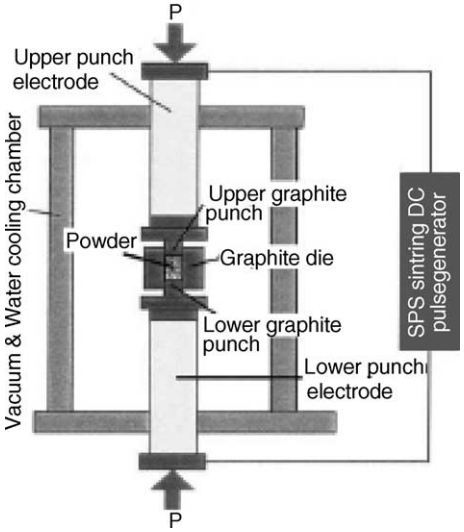

Fig. 1. Schematic of the SPS system configuration.

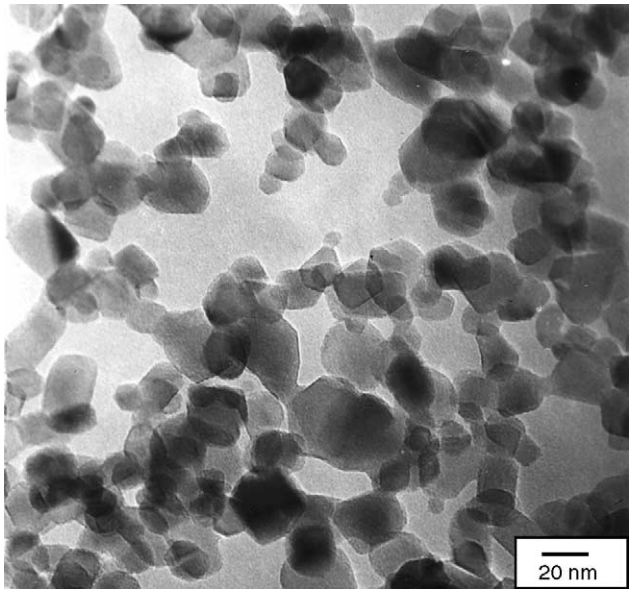

Fig. 2. The TEM image of $La_2Mo_2O_9$ ultrafine powder.

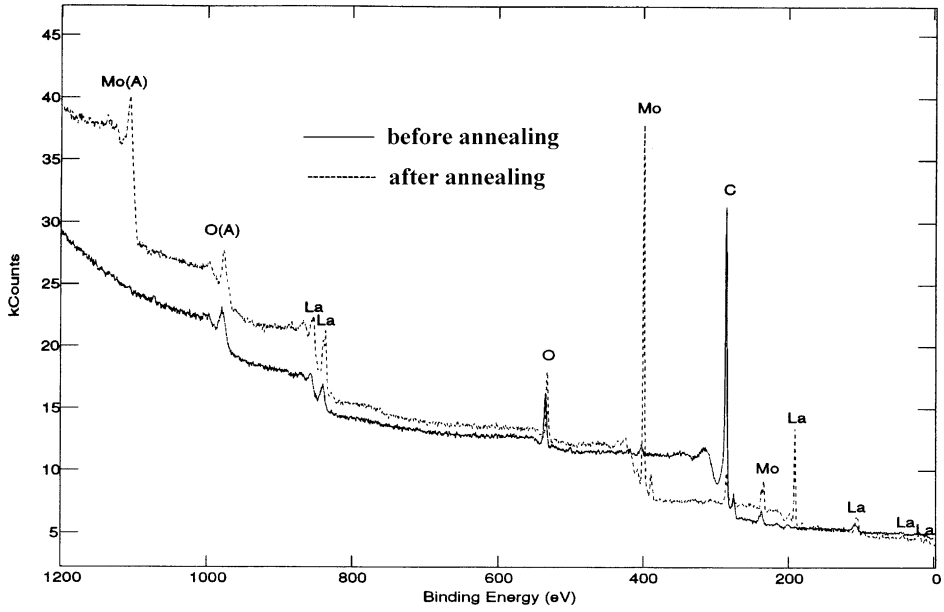

Fig. 3. The X-ray photoelectron spectra for as-sintered SPS $La_2Mo_2O_9$ specimens before and after annealing at 700 °C.

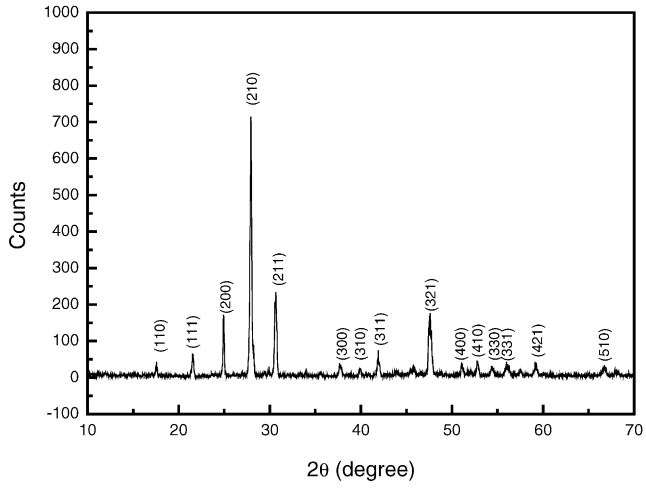

Fig. 4. The XRD pattern of the annealed SPS $La_2Mo_2O_9$ specimen.

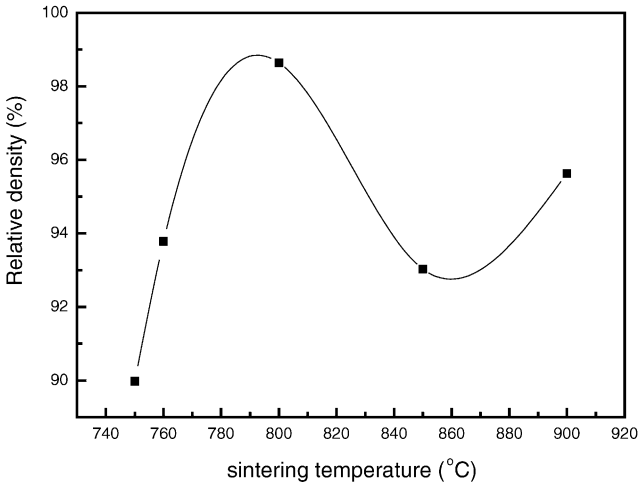

Fig. 5. The relationship between the relative density and sintering temperature of SPS for $La_2Mo_2O_9$ specimen (with holding time of 5 min).

specimen was shown in Fig. 4, no other phase except for $La_2Mo_2O_9$ was found.

The relative densities of the specimens prepared under different sintering conditions were listed in Table 1. It was clearly shown that much higher relative density by SPS could be obtained in comparison with the conventional sintering method. In addition, SPS effectively accelerated the sintering process and shortened the process from several hours for conventional sintering to a few minutes. Fig. 5 showed the re-

Table 1
The relative density of $La_2Mo_2O_9$ specimens obtained by SPS sintering under different conditions and by conventional sintering

Sample name	Sinter method	Sintering temperature (°C)	Holding time (min)	Relative density (%)
SPS 1	SPS	900	30	96.05
SPS 2	SPS	900	5	95.63
SPS 3	SPS	900	0	90.21
SPS 4	SPS	850	5	93.03
SPS 5	SPS	800	5	98.64
SPS 6	SPS	750	5	89.98
Con7	Conventional	500/10 h–900/12 h		77.67

lationship between the sintering temperature and relative density of specimens sintered for 5 min. As can be seen in Fig. 5, with the increase of sintering temperature the relative density of the specimen increased. At 800 °C, the relative density reached the highest value 98.64%, then it decreased. While at 900 °C, the relative density increased again. As shown in Table 1, the holding time at a SPS sintering temperature of 900 °C also affected the densities of the specimens. A relative density of 90.21% was obtained for sample without holding at the sintering temperature. When the holding time increased to 5 min, the relative density of the specimen reached 95.63%. Further prolonging the holding to 30 min, the relative density reached 96.05%. A sufficient holding time for SPS was necessary to get well-sintered specimens.

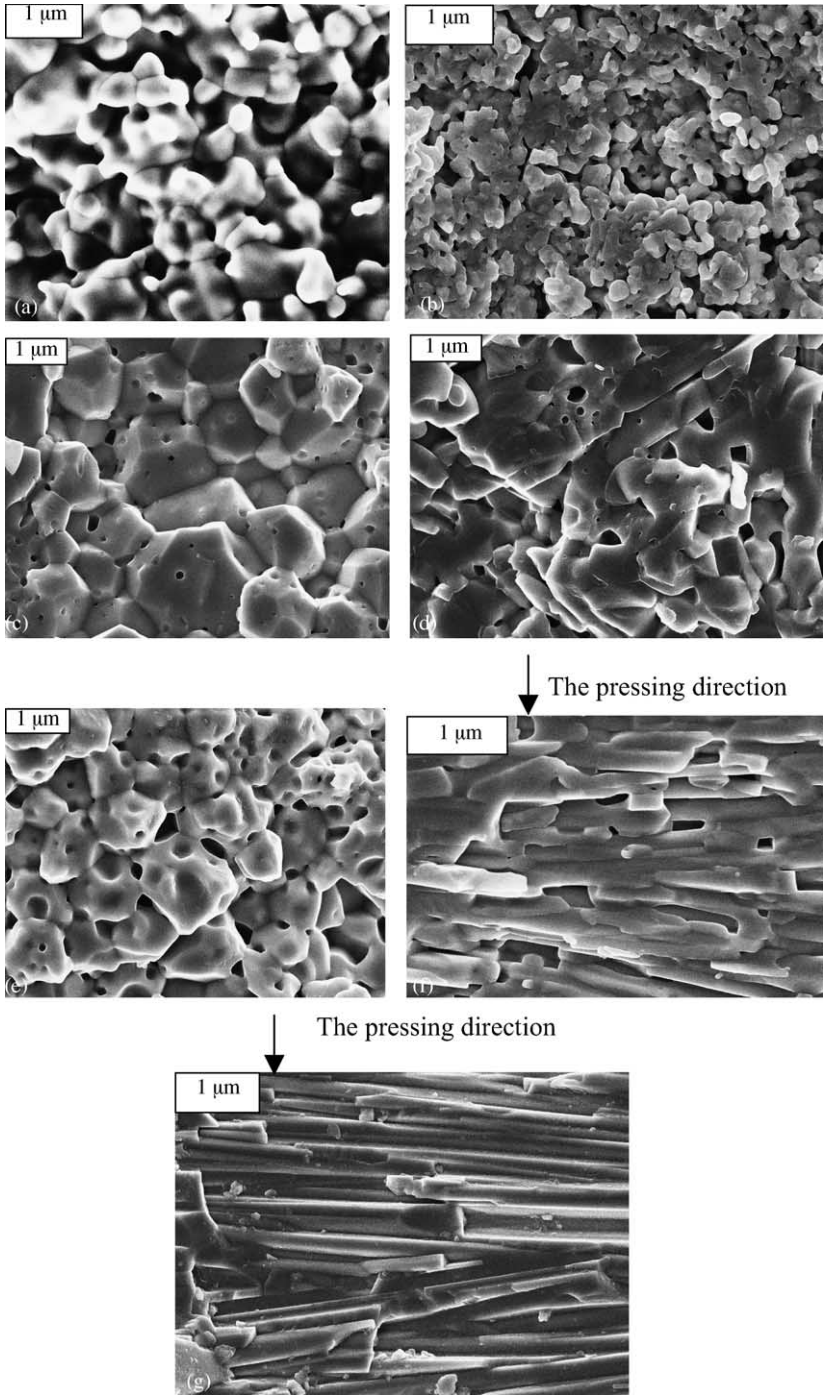

Fig. 6. The SEM images of the fracture section of $La_2Mo_2O_9$ specimens sintered by conventional sintering and SPS under different conditions. (a) By conventional sintering; (b) by SPS at 750 °C for 5 min; (c) by SPS at 800 °C for 5 min; (d) by SPS at 850 °C for 5 min; (e) by SPS at 900 °C for 0 min; (f) by SPS at 900 °C for 5 min; and (g) by SPS at 900 °C for 30 min.

Fig. 6 showed the SEM images of the fractured sections of the specimens sintered by conventional sintering and SPS at different temperatures and for different time. As shown in Fig. 6a, large pores were observed both at the grain boundaries and within the grains in the conventionally sintered specimen, indicating that the specimen was not really dense. For SPS specimens sintered at 750 °C, the grain size was about 300–500 nm and many pores were observed at the grain boundaries (Fig. 6b). It appeared that the specimen was not sintered well. The relative density of the ceramics was lower than 90%, leading to a loose and brittle feature of the specimen. The grains sintered at 800 °C were round or hexagonal in morphology with the grain size increased to 1–3 μm, moreover the grain boundary became very narrow and only a small number of pores were observed in the grains (Fig. 6c). Therefore, its relative density was very high. Fig. 6e showed the SEM image for the specimen sintered at 900 °C without holding time. Many pores were observed in the sample both at the grain boundaries and within the grains. As mentioned above, the specimen was not well sintered and with lower density.

An interesting and greatly changed microstructure was observed in the specimen sintered at 900 °C for 5 min. The grains in the specimen became long and rod-type. The direction of the parallelly aligned rod-grains was vertical to the pressing direction on specimen during sintering (Fig. 6f). Small amounts of pores were observed between the elongated grains, which resulted in the decrease of its relative density to some extent. These rod-type grains were found to be as long as 8 μm or longer. Further increase of holding time at 900 °C to 30 min led to the rod-type grains longer than 15 μm and more closely packed (Fig. 6g), which resulted in increased relative density of the specimen. However, overlapping of the rod-type grains would happen as can be seen in Fig. 6g, which caused the density of the specimen to be lower than that of the specimen without the rod-type feature. At a lower sintering temperature 850 °C, some long grains started to appear along with round grains (Fig. 6d). The coexistence of the two kinds of grains with completely different morphologies resulted in more pores at the grain boundaries, which could be the reason why the relative density decreased rather than increased while the sintering temperature was raised to 850 °C.

In flowing air or pure oxygen atmosphere, comparable conductivity values were obtained for the specimens, which indicated that within the oxygen partial pressure range, the conductivity was predominantly ionic in nature.[9,16] The ionic conductivities of the specimens sintered by conventional and SPS procedures at different temperatures were shown in Fig. 7. Usually, the higher relative density of the specimen, the higher was the ionic conductivity. But, an abnormal phenomenon was observed with the specimen sintered at 900 °C for 30 min. The ionic conductivity perpendicular to the direction of rod-type grain alignment was higher than that of the specimen sintered at 800 °C for 5 min which had the highest density. It suggested that regularly and very closely aligned rod-type grains would effectively improve the compactness

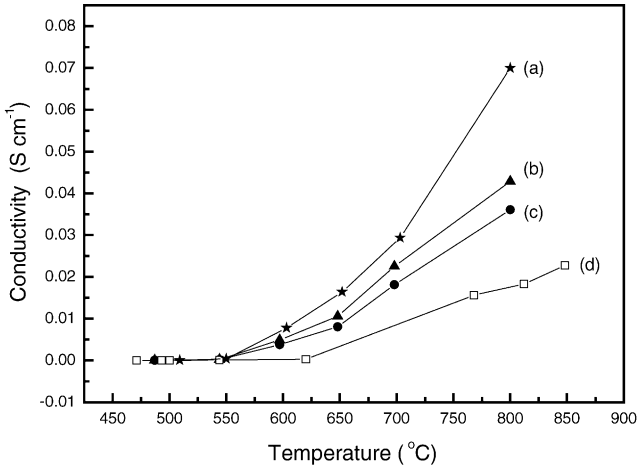

Fig. 7. The ionic conductivity at different temperatures for the $La_2Mo_2O_9$ specimens derived from conventional and SPS sintering. (a) Specimen sintered by SPS at 900 °C for 30 min; (b) by SPS at 800 °C for 5 min; (c) by SPS at 850 °C for 5 min; and (d) by conventional sintering.

of the specimen, and therefore very helpful to the transport of oxygen ions between grains and reduce the resistance at grain boundaries. Fig. 8 shows the comparison of the ionic conductivities measured parallel and perpendicular to the direction of rod-type grain alignment for the specimens sintered by SPS at 900 °C for 5 and 30 min, respectively. Obvious anisotropy of the ionic conductivity was observed with the conductivity value parallel to the direction of rod-type grains higher than that perpendicular to the rod-type grains. Fig. 8 also shows that the ionic conductivity of specimens sintered at 900 °C for 30 min was higher than that of specimens for 5 min, which also demonstrated the effect of compaction on the ionic conductivity. The effect was further confirmed by the comparison of the conductivity of grain boundaries of the specimens sintered by both SPS and conventional method as shown in Fig. 9 and in Table 2.

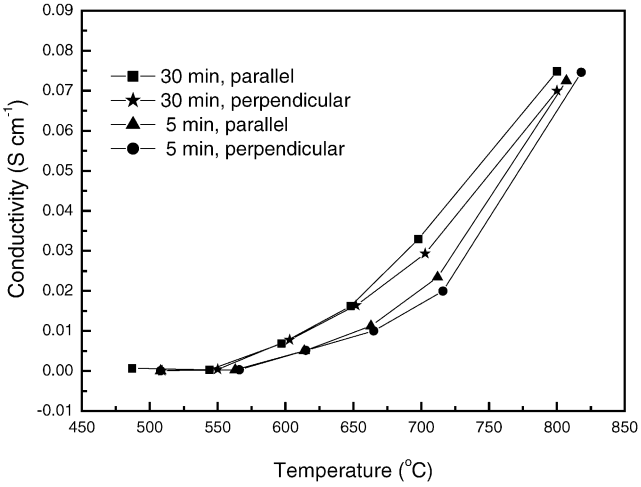

Fig. 8. The comparison of ionic conductivities at different temperatures measured parallel or perpendicular to the rod-type grains in the specimens sintered by SPS at 900 °C for 30 and 5 min, respectively.

Table 2
The comparison of the conductivities of grains and grain boundary for the specimens sintered by conventional sintering and SPS at 900 °C for 5 min

Samples	Conductivity of grain (S cm^{-1})		Conductivity of grain boundary (S cm^{-1})	
	712 °C	660 °C	712 °C	660 °C
SPS sintered				
Longitudinal direction	0.02358	0.01132	0.43262	0.1530
Transverse direction	0.02294	0.01464	0.1030	0.03069
Conventionally sintered	0.01925	0.01251	0.08345	0.01325

According to the Ref. 17, the resistance of oxygen ions transported through the electrolyte can be expressed as followings:

$$R = R_g + R_{gb} = \frac{L\rho_g}{S} + \frac{L\rho_{gb}}{S} \quad (1)$$

where R, R_g and R_{gb} are the electrical resistance of whole electrolyte, grain and grain boundary, respectively, L and S are the geometric surface area and thickness of the electrolyte, ρ_g and ρ_{gb} are the apparent resistivity of grain and grain boundary based on the geometric dimension. Therefore, the apparent ionic conductivity of grain and grain boundary σ_g, σ_{gb} can be calculated from Eq. (1).

As listed in Table 2, the intragranular ionic conductivities in both directions for the specimen by SPS at 900 °C for 5 min, which owned the microstructure of Fig. 6f, were similar and comparable to those of the conventionally sintered specimen. However, the contribution of the grain boundary conductivity of the SPS specimen with long rod-type grains was much higher than that of the conventionally sintered specimen. Moreover, the conductivity of grain boundary parallel to the direction of rod-type grains was four to five times higher than the perpendicular results. As known, the intragranular conductivity is dependent on the crystal structure of the material, therefore all the conductivities of grain measured above are similar. However, the conductivity of grain boundary was relative to compactness of specimen, pores between grains and so on. In a normal sintered ceramic $La_2Mo_2O_9$ specimen with such microstructure as shown in Fig. 7c, the conductivities of grain boundaries should be similar in all direction. However, for the specimen with anisotropical microstructure as shown in Fig. 6f and g, the structure, interface and pores between the grains in different directions were different. Obviously, there were many more interfaces and possible pores perpendicular to the direction of rod-type grains than those parallel to the direction of the grains. So the conductivity of grain boundaries measured parallel to the direction of grains was higher than the perpendicular direction, which resulted in ionic conductivity anisotropy, with the conductivity value parallel to the direction of rod-type grains higher than the perpendicular direction in Fig. 8.

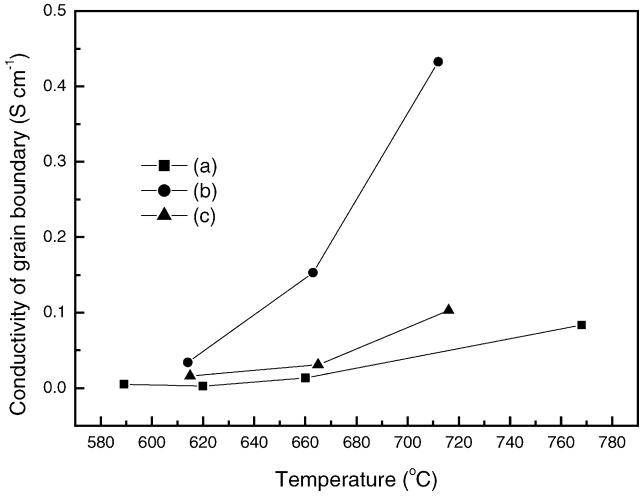

Fig. 9. The comparison of ionic conductivities of grain boundary at different temperatures for the specimen sintered by SPS for 5 min, measured parallel (a) or perpendicular (b) to the rod-type grains and the specimen sintered by conventional sintering (c).

4. Conclusions

In this work, the dense $La_2Mo_2O_9$ ceramic electrolytes were prepared with ultrafine powder by SPS rapid sintering method. The conductivity of the specimens sintered by SPS was much higher than those sintered by conventional processing. Moreover, the unilateral alignment of rod-type grains happened in the specimens sintered by SPS at higher temperatures or for longer holding time. The anisotropy in ionic conductivity was determined and attribute to the directional alignment of rod-type grains. The oxygen ionic conductivity parallel to the direction of rod-type grains was higher than that perpendicular to the grains.

Acknowledgement

This work was financially supported by the key project of Nature Science Foundation of China (NSFC) No. 20333040.

References

1. Yahiro, H., Ohuchi, T. and Eguchi, K., *J. Mater. Sci.*, 1998, **23**, 1036.
2. Minh, N. Q., *J. Am. Ceram. Soc.*, 1993, **76**, 563.
3. Kendall, K. R., Navas, C., Thomas, J. K. and Kilner, J. A., *Solid State Ionics*, 2000, **13**, 129.
4. Kilner, J. A., *Solid State Ionics*, 2000, **129**, 13.
5. Takahashi, T. and Iwara, H., *J. Appl. Electrochem.*, 1973, **3**, 65.
6. Ishihara, T., Matsuda, H. and Takita, Y., *J. Am. Chem. Soc.*, 1994, **26**, 3801.

7. Abraham, F., Debreuille-Gresse, M., Mairesse, G. and Nowogrocki, G., *Solid State Ionics*, 1988, **28–30**, 5529.
8. Tuller, H. L., *Solid State Ionics*, 1997, **94**, 63–74.
9. Lacorre, P., Goutenoire, F., Bohnke, O., Retoux, R. and Laligant, Y., *Nature*, 2000, **404**, 856.
10. Kuang, W., Fan, Y., Qiu, J. and Chen, Y., *J. Mater. Chem. Commun.*, 1998, **8**(1), 19–20.
11. Lacorre, P. and Retoux, R., *J. Solid State Chem.*, 1997, **132**, 443–446.
12. Goutenoir, F., Isnard, O., Suard, E., Bohnke, O., Laligant, Y., Retoux, R. and Lacorre, P., *J. Mater. Chem.*, 2001, **11**, 119–124.
13. Li, W. and Gao, L., *J. Eur. Ceram. Soc.*, 2000, **20**, 2441–2445.
14. Khor, K., Yu, L., Chan, S. and Chen, X., *J. Eur. Ceram. Soc.*, 2003, **20**, 1855–1863.
15. Khor, K., Cheng, K., Yu, L. and Boey, F., *Mater. Sci. Eng. A*, 2003, **347**, 300.
16. Yang, J., Gu, Z., Wen, Z. and Yan, D., Preparation and characterization of solid electrolytes $La_{2-x}A_xMo_{2-y}W_yO_9$ (A = Sm, Bi). *Solid State Ionics* (in press).
17. Chen, X., Khor, K., Chan, S. and Yu, L., *Mater. Sci. Eng. A*, 2003, **341**, 43.